

## Warning Concerning Copyright Restrictions

The Copyright Law of the United States (Title 17, United States Code) governs the making of photocopies or other reproductions of copyrighted materials.

Under certain conditions specified in the law, libraries and archives are authorized to furnish a photocopy or other reproduction. One of these specified conditions is that the photocopy or reproduction is not to be used for any purpose other than private study, scholarship, or research. If electronic transmission of reserve material is used for purposes in excess of what constitutes "fair use," that user may be liable for copyright infringement.

University of Nevada, Reno

**Characterization of Smooth Muscle Myosin Light Chain Kinase Using  
Crystallization and Transient Kinetics**

A thesis submitted in partial fulfillment  
of the requirements for the degree of

Bachelor of Science in Biochemistry and Molecular Biology and the Honors Program

by

Jason H. Phan

Dr. Patricia Ellison, Thesis Advisor

May 2015

**UNIVERSITY  
OF NEVADA  
RENO**

**THE HONORS PROGRAM**

We recommend that the thesis  
prepared under our supervision by

Jason Phan

entitled

**Characterization of Smooth Muscle Myosin Light Chain Kinase Using  
Crystallization and Transient Kinetics**

be accepted in partial fulfillment of the  
requirements for the degree of

**Bachelor of Science in Biochemistry and Molecular Biology**

---

Patricia Ellison, Ph.D., Thesis Advisor

---

Tamara Valentine, Ph. D., Director, Honors Program

May 2015

## **Abstract**

Crystallization experiments and transient kinetic methods were used to characterize the first 75 amino acid segment of smooth muscle myosin light chain kinase (MLCK N1-75). As of now, the exact mechanism by which MLCK interacts with actomyosin complexes in smooth muscle is not well-understood because there is no high-resolution 3-dimensional structure of MLCK available. In this project, the crystallization of the actin-binding domain of MLCK (called N1-75) with glutathione S-transferase (GST) was attempted in order to provide such a model. Polyethylene glycol and ammonium sulfate, within a pH range of 6.5 to 8.0, seemed to be the most promising precipitants to induce crystallization. Observation of crystallization setups with these parameters showed no definitive results, and crystallization was not successful. Future experiments should attempt to increase protein quality before crystallization by removing the GST tag and achieving higher protein concentration. In addition to the crystallization experiments, transient kinetic methods were used to characterize MLCK N1-75 interactions with actin and smooth muscle myosin subfragment 1 (S1). It was found that MLCK N1-75, when mixed with actin, decreased the rate at which actin binds S1. This data suggests that MLCK N1-75 may be competing with S1 for the same binding site on actin.

## Table of Contents

Abstract .....	i
Table of Contents .....	ii
Introduction .....	1
Methods .....	2
Results .....	9
Discussion .....	15
References .....	18

## Introduction

Smooth muscle is found in the walls of blood vessels, the gastrointestinal tract, the respiratory tract, and many other areas in the body. Poor regulation of smooth muscle results in abnormal contraction, which can lead to a diverse range of health conditions including asthma and cardiovascular disease (Leguillette *et al.*, 2009) (Yuan *et al.*, 2014). Smooth muscle contraction is regulated by phosphorylation of the regulatory light chain of myosin II by myosin light chain kinase (MLCK) (Adelstein & Klee, 1981). The structurally complex MLCK contains multiple domains that each contribute to its function as a kinase (Hong *et al.*, 2011). Currently, there is no high resolution 3-dimensional structure of MLCK. The successful crystallization and x-ray crystallographic analysis of MLCK would serve as the basis for understanding the exact mechanism by which MLCK interacts with actomyosin complexes in smooth muscle.

MLCK is a long and flexible protein: it contains at least seven domains for binding to myosin, actin, and calmodulin as shown in Figure 1 (Hong *et al.*, 2011). The sheer size of MLCK makes it unfeasible to crystallize the entire protein all at once; therefore, the focus of this research will be on the first 75 residues of the amino terminus which is thought to contain an actin-binding domain (referred to as MLCK N1-75). Prior research has shown that MLCK N1-75 is necessary and sufficient for high affinity binding to actin due to three DFRxxL motifs (Smith *et al.*, 1999). Binding to actin allows MLCK to stay localized to myofilaments so that the enzyme can rapidly phosphorylate myosin to induce contraction (Smith & Stull, 2000). It also anchors MLCK so that the enzyme does not sterically hinder myosin during contraction. Transient kinetic methods using stopped-flow spectroscopy will be used to further characterize MLCK N1-75

interactions with actin. Specifically, it will be tested whether or not MLCK N1-75 competes with smooth muscle myosin subfragment 1 (S1) for the same binding site on actin. This thesis reports the purification of MLCK N1-75, the crystallization experiments, and the actin:N1-75 binding studies.

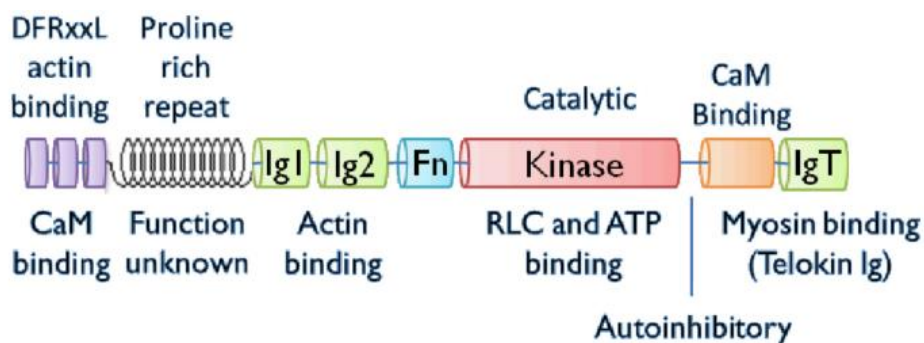


**Figure 1. Domain structure of smooth muscle MLCK (from Hong *et al.*, 2011)**  
The focus of this research is on the N1-75 segment of MLCK which constitutes the DFRxxL actin binding domain.

## Methods

### CRYSTALLIZATION

#### Preparation of MLCK N1-75

MLCK N1-75 with glutathione S-transferase (GST) was expressed using *E. coli* in Dr. Christine Cremo's lab. Cells from a transformed stock were plated and incubated at 37°C overnight. Viable colonies were selected and transferred into fresh LB broth. Cells were allowed to grow until an OD reading of approximately 0.4. Cells were induced to a final concentration of 0.1mM IPTG. Cells were lysed using lysozyme. DTT was added to a final concentration of 5mM. Cells were spun at 100K rpm for 30min. The collected supernatant contained MLCK N1-75 GST. The GST affinity tag allowed it to be purified

using glutathione affinity chromatography on the ÄKTA pure FPLC (fast protein liquid chromatography) system. The MLCK N1-75 GST lysate was injected into GE's GSTPrep FF 16/10 column. The column required phosphate buffered saline as the binding buffer. Once the lysate was pushed through the column (and all of the waste was eluted), a glutathione elution buffer was used to elute MLCK N1-75 GST from the column (Fig. 2a). The fractions containing the protein were pooled and concentrated by precipitation with 70% ammonium sulfate and re-suspending and dialyzing in HMM buffer. Gel electrophoresis was conducted to verify that the size of the collected protein was approximately 37kDa (Fig. 2b).

### **Initial Crystallization Setups**

After purification, MLCK N1-75 GST was placed into hanging drop vapor diffusion setups to induce supersaturation and crystallization (McPherson & Gavira, 2013). The Crystal Screen kits from Hampton Research were used for the five crystallization plates labeled N75-GST 1 through 5, respectively. The kits contain sparse matrix screens which sample a variety of salts, polymers, organics, and pH levels (see Tab. 1 for reagent formulations). The crystallization setups were stored at 4°C and left to equilibrate against the reservoir solution. Growth patterns of each setup were routinely observed using light microscopy.

**Table 1. Hampton Research Crystal Screens 1 and 2 reagent formulations**

For the initial screens, 98 hanging drop setups were made to accommodate all of the reagents in the Hampton Research kits.

Crystal Screen™		HR2-110 Reagent Formulation			
Tube #	Salt	Tube #	Buffer ◊	Tube #	Precipitant
1.	0.02 M Calcium chloride dihydrate	1.	0.1 M Sodium acetate trihydrate pH 4.6	1.	30% v/v (+/-)-2-Methyl-2,4-pentanediol
2.	None	2.	None	2.	0.4 M Potassium sodium tartrate tetrahydrate
3.	None	3.	None	3.	0.4 M Ammonium phosphate monobasic
4.	None	4.	0.1 M TRIS hydrochloride pH 8.5	4.	2.0 M Ammonium sulfate
5.	0.2 M Sodium citrate tribasic dihydrate	5.	0.1 M HEPES sodium pH 7.5	5.	30% v/v (+/-)-2-Methyl-2,4-pentanediol
6.	0.2 M Magnesium chloride hexahydrate	6.	0.1 M TRIS hydrochloride pH 8.5	6.	30% w/v Polyethylene glycol 4,000
7.	None	7.	0.1 M Sodium cacodylate trihydrate pH 6.5	7.	1.4 M Sodium acetate trihydrate
8.	0.2 M Sodium citrate tribasic dihydrate	8.	0.1 M Sodium cacodylate trihydrate pH 6.5	8.	30% v/v 2-Propanol
9.	0.2 M Ammonium acetate	9.	0.1 M Sodium citrate tribasic dihydrate pH 5.6	9.	30% w/v Polyethylene glycol 4,000
10.	0.2 M Ammonium acetate	10.	0.1 M Sodium acetate trihydrate pH 4.6	10.	30% w/v Polyethylene glycol 4,000
11.	None	11.	0.1 M Sodium citrate tribasic dihydrate pH 5.6	11.	1.0 M Ammonium phosphate monobasic
12.	0.2 M Magnesium chloride hexahydrate	12.	0.1 M HEPES sodium pH 7.5	12.	30% v/v 2-Propanol
13.	0.2 M Sodium citrate tribasic dihydrate	13.	0.1 M TRIS hydrochloride pH 8.5	13.	30% v/v Polyethylene glycol 400
14.	0.2 M Calcium chloride dihydrate	14.	0.1 M HEPES sodium pH 7.5	14.	28% v/v Polyethylene glycol 400
15.	0.2 M Ammonium sulfate	15.	0.1 M Sodium cacodylate trihydrate pH 6.5	15.	30% w/v Polyethylene glycol 8,000
16.	None	16.	0.1 M HEPES sodium pH 7.5	16.	1.5 M Lithium sulfate monohydrate
17.	0.2 M Lithium sulfate monohydrate	17.	0.1 M TRIS hydrochloride pH 8.5	17.	30% w/v Polyethylene glycol 4,000
18.	0.2 M Magnesium acetate tetrahydrate	18.	0.1 M Sodium cacodylate trihydrate pH 6.5	18.	20% w/v Polyethylene glycol 8,000
19.	0.2 M Ammonium acetate	19.	0.1 M TRIS hydrochloride pH 8.5	19.	30% v/v 2-Propanol
20.	0.2 M Ammonium sulfate	20.	0.1 M Sodium acetate trihydrate pH 4.6	20.	25% w/v Polyethylene glycol 4,000
21.	0.2 M Magnesium acetate tetrahydrate	21.	0.1 M Sodium cacodylate trihydrate pH 6.5	21.	30% v/v (+/-)-2-Methyl-2,4-pentanediol
22.	0.2 M Sodium acetate trihydrate	22.	0.1 M TRIS hydrochloride pH 8.5	22.	30% w/v Polyethylene glycol 4,000
23.	0.2 M Magnesium chloride hexahydrate	23.	0.1 M HEPES sodium pH 7.5	23.	30% v/v Polyethylene glycol 400
24.	0.2 M Calcium chloride dihydrate	24.	0.1 M Sodium acetate trihydrate pH 4.6	24.	20% v/v 2-Propanol
25.	None	25.	0.1 M Imidazole pH 6.5	25.	1.0 M Sodium acetate trihydrate
26.	0.2 M Ammonium acetate	26.	0.1 M Sodium citrate tribasic dihydrate pH 5.6	26.	30% v/v (+/-)-2-Methyl-2,4-pentanediol
27.	0.2 M Sodium citrate tribasic dihydrate	27.	0.1 M HEPES sodium pH 7.5	27.	20% v/v 2-Propanol
28.	0.2 M Sodium acetate trihydrate	28.	0.1 M Sodium cacodylate trihydrate pH 6.5	28.	30% w/v Polyethylene glycol 8,000
29.	None	29.	0.1 M HEPES sodium pH 7.5	29.	0.8 M Potassium sodium tartrate tetrahydrate
30.	0.2 M Ammonium sulfate	30.	None	30.	30% w/v Polyethylene glycol 8,000
31.	0.2 M Ammonium sulfate	31.	None	31.	30% w/v Polyethylene glycol 4,000
32.	None	32.	None	32.	2.0 M Ammonium sulfate
33.	None	33.	None	33.	4.0 M Sodium formate
34.	None	34.	0.1 M Sodium acetate trihydrate pH 4.6	34.	2.0 M Sodium formate
35.	None	35.	0.1 M HEPES sodium pH 7.5	35.	0.8 M Sodium phosphate monobasic monohydrate 0.8 M Potassium phosphate monobasic
36.	None	36.	0.1 M TRIS hydrochloride pH 8.5	36.	8% w/v Polyethylene glycol 8,000
37.	None	37.	0.1 M Sodium acetate trihydrate pH 4.6	37.	8% w/v Polyethylene glycol 4,000
38.	None	38.	0.1 M HEPES sodium pH 7.5	38.	1.4 M Sodium citrate tribasic dihydrate
39.	None	39.	0.1 M HEPES sodium pH 7.5	39.	2% v/v Polyethylene glycol 400 2.0 M Ammonium sulfate
40.	None	40.	0.1 M Sodium citrate tribasic dihydrate pH 5.6	40.	20% v/v 2-Propanol 20% w/v Polyethylene glycol 4,000
41.	None	41.	0.1 M HEPES sodium pH 7.5	41.	10% v/v 2-Propanol 20% w/v Polyethylene glycol 4,000
42.	0.05 M Potassium phosphate monobasic	42.	None	42.	20% w/v Polyethylene glycol 8,000
43.	None	43.	None	43.	30% w/v Polyethylene glycol 1,500
44.	None	44.	None	44.	0.2 M Magnesium formate dihydrate
45.	0.2 M Zinc acetate dihydrate	45.	0.1 M Sodium cacodylate trihydrate pH 6.5	45.	18% w/v Polyethylene glycol 8,000
46.	0.2 M Calcium acetate hydrate	46.	0.1 M Sodium cacodylate trihydrate pH 6.5	46.	18% w/v Polyethylene glycol 8,000
47.	None	47.	0.1 M Sodium acetate trihydrate pH 4.6	47.	2.0 M Ammonium sulfate
48.	None	48.	0.1 M TRIS hydrochloride pH 8.5	48.	2.0 M Ammonium phosphate monobasic
49.	1.0 M Lithium sulfate monohydrate	49.	None	49.	2% w/v Polyethylene glycol 8,000
50.	0.5 M Lithium sulfate monohydrate	50.	None	50.	15% w/v Polyethylene glycol 8,000

◊ Buffer pH is that of a 1.0 M stock prior to dilution with other reagent components: pH with HCl or NaOH.

## Crystal Screen 2™

## HR2-112 Reagent Formulation

Tube #	Salt	Tube #	Buffer ◊	Tube #	Precipitant
1.	2.0 M Sodium chloride	1.	None	1.	10% w/v Polyethylene glycol 6,000
2.	0.5 M Sodium chloride	2.	None	2.	0.01 M Hexadecyltrimethylammonium bromide
	0.01 M Magnesium chloride hexahydrate				
3.	None	3.	None	3.	25% v/v Ethylene glycol
4.	None	4.	None	4.	35% v/v 1,4-Dioxane
5.	2.0 M Ammonium sulfate	5.	None	5.	5% v/v 2-Propanol
6.	None	6.	None	6.	1.0 M Imidazole pH 7.0
7.	None	7.	None	7.	10% w/v Polyethylene glycol 1,000 10% w/v Polyethylene glycol 8,000
8.	1.5 M Sodium chloride	8.	None	8.	10% v/v Ethanol
9.	None	9.	0.1 M Sodium acetate trihydrate pH 4.6	9.	2.0 M Sodium chloride
10.	0.2 M Sodium chloride	10.	0.1 M Sodium acetate trihydrate pH 4.6	10.	30% v/v (+/-)-2-Methyl-2,4-pentanediol
11.	0.01 M Cobalt(II) chloride hexahydrate	11.	0.1 M Sodium acetate trihydrate pH 4.6	11.	1.0 M 1,6-Hexanediol
12.	0.1 M Cadmium chloride hydrate	12.	0.1 M Sodium acetate trihydrate pH 4.6	12.	30% v/v Polyethylene glycol 400
13.	0.2 M Ammonium sulfate	13.	0.1 M Sodium acetate trihydrate pH 4.6	13.	30% w/v Polyethylene glycol monomethyl ether 2,000
14.	0.2 M Potassium sodium tartrate tetrahydrate	14.	0.1 M Sodium citrate tribasic dihydrate pH 5.6	14.	2.0 M Ammonium sulfate
15.	0.5 M Ammonium sulfate	15.	0.1 M Sodium citrate tribasic dihydrate pH 5.6	15.	1.0 M Lithium sulfate monohydrate
16.	0.5 M Sodium chloride	16.	0.1 M Sodium citrate tribasic dihydrate pH 5.6	16.	2% v/v Ethylene imine polymer
17.	None	17.	0.1 M Sodium citrate tribasic dihydrate pH 5.6	17.	35% v/v tert-Butanol
18.	0.01 M Iron(III) chloride hexahydrate	18.	0.1 M Sodium citrate tribasic dihydrate pH 5.6	18.	10% v/v Jeffamine® M-600®
19.	None	19.	0.1 M Sodium citrate tribasic dihydrate pH 5.6	19.	2.5 M 1,6-Hexanediol
20.	None	20.	0.1 M MES monohydrate pH 6.5	20.	1.6 M Magnesium sulfate heptahydrate
21.	0.1 M Sodium phosphate monobasic monohydrate 0.1 M Potassium phosphate monobasic	21.	0.1 M MES monohydrate pH 6.5	21.	2.0 M Sodium chloride
22.	None	22.	0.1 M MES monohydrate pH 6.5	22.	12% w/v Polyethylene glycol 20,000
23.	1.6 M Ammonium sulfate	23.	0.1 M MES monohydrate pH 6.5	23.	10% v/v 1,4-Dioxane
24.	0.05 M Cesium chloride	24.	0.1 M MES monohydrate pH 6.5	24.	30% v/v Jeffamine® M-600®
25.	0.01 M Cobalt(II) chloride hexahydrate	25.	0.1 M MES monohydrate pH 6.5	25.	1.8 M Ammonium sulfate
26.	0.2 M Ammonium sulfate	26.	0.1 M MES monohydrate pH 6.5	26.	30% w/v Polyethylene glycol monomethyl ether 5,000
27.	0.01 M Zinc sulfate heptahydrate	27.	0.1 M MES monohydrate pH 6.5	27.	25% v/v Polyethylene glycol monomethyl ether 550
28.	None	28.	None	28.	1.6 M Sodium citrate tribasic dihydrate pH 6.5
29.	0.5 M Ammonium sulfate	29.	0.1 M HEPES pH 7.5	29.	30% v/v (+/-)-2-Methyl-2,4-pentanediol
30.	None	30.	0.1 M HEPES pH 7.5	30.	10% w/v Polyethylene glycol 6,000 5% v/v (+/-)-2-Methyl-2,4-pentanediol
31.	None	31.	0.1 M HEPES pH 7.5	31.	20% v/v Jeffamine® M-600®
32.	0.1 M Sodium chloride	32.	0.1 M HEPES pH 7.5	32.	1.6 M Ammonium sulfate
33.	None	33.	0.1 M HEPES pH 7.5	33.	2.0 M Ammonium formate
34.	0.05 M Cadmium sulfate hydrate	34.	0.1 M HEPES pH 7.5	34.	1.0 M Sodium acetate trihydrate
35.	None	35.	0.1 M HEPES pH 7.5	35.	70% v/v (+/-)-2-Methyl-2,4-pentanediol
36.	None	36.	0.1 M HEPES pH 7.5	36.	4.3 M Sodium chloride
37.	None	37.	0.1 M HEPES pH 7.5	37.	10% w/v Polyethylene glycol 8,000 8% v/v Ethylene glycol
38.	None	38.	0.1 M HEPES pH 7.5	38.	20% v/v Polyethylene glycol 10,000
39.	0.2 M Magnesium chloride hexahydrate	39.	0.1 M Tris pH 8.5	39.	3.4 M 1,6-Hexanediol
40.	None	40.	0.1 M Tris pH 8.5	40.	25% v/v tert-Butanol
41.	0.01 M Nickel(II) chloride hexahydrate	41.	0.1 M Tris pH 8.5	41.	1.0 M Lithium sulfate monohydrate
42.	1.5 M Ammonium sulfate	42.	0.1 M Tris pH 8.5	42.	12% v/v Glycerol
43.	0.2 M Ammonium phosphate monobasic	43.	0.1 M Tris pH 8.5	43.	50% v/v (+/-)-2-Methyl-2,4-pentanediol
44.	None	44.	0.1 M Tris pH 8.5	44.	20% v/v Ethanol
45.	0.01 M Nickel(II) chloride hexahydrate	45.	0.1 M Tris pH 8.5	45.	20% w/v Polyethylene glycol monomethyl ether 2,000
46.	0.1 M Sodium chloride	46.	0.1 M BICINE pH 9.0	46.	20% v/v Polyethylene glycol monomethyl ether 550
47.	None	47.	0.1 M BICINE pH 9.0	47.	2.0 M Magnesium chloride hexahydrate
48.	None	48.	0.1 M BICINE pH 9.0	48.	2% v/v 1,4-Dioxane 10% w/v Polyethylene glycol 20,000










◊ Buffer pH is that of a 1.0 M (0.5 M for MES monohydrate) stock prior to dilution with other reagent components: pH with HCl or NaOH.

## Optimized Crystallization Setups

Crystallization experiments were evaluated using a scale ranging from 1 (clear, no precipitate, no crystals) to 9 (large crystals) (Tab. 2). Conditions that produced heavy precipitate were eliminated from future experiments. After observing each hanging drop in the initial crystal screens, new crystallization setups were made using optimized parameters. Observation of protein precipitation in the initial setups showed that a pH range of 6.5 to 7.5 with polyethylene glycol or ammonium sulfate as the precipitant seemed most likely to induce crystal growth (Tab. 3). Five crystallization plates with optimized parameters were created (Tab. 4). The first three (labeled N75-GST 6, 7, & 8 respectively) used varying polymer lengths and concentrations of polyethylene glycol as the precipitant. The next two (N75-GST 9 & 10) used varying concentrations of ammonium sulfate as the precipitant and sodium chloride as an added salt. All of these setups were kept at 4°C and within a pH range of 6.5 to 8.0 in 0.1M HEPES buffer. These hanging drop setups were left to equilibrate, and they were periodically observed using light microscopy. The crystallization parameters resulting in the most promising observations are shown in Table 5.

**Table 2. Scoring scale for crystallization setups**

This scale ranks typical observations in crystallization experiments (images from Hampton Research Crystal Screen User Guide).

Score	Observation	Example
1	Clear drop	
2	Phase separation	
3	Regular granular precipitate	
4	Birefringent precipitate or microcrystals	
5	Posettes or spherulites	
6	Needles (1D growth)	
7	Plates (2D growth)	
8	Single crystals (3D growth < 0.2mm)	
9	Single crystals (3D growth >0.2mm)	

## **TRANSIENT KINETICS**

### **Preparation of Proteins**

MLCK N1-75, pyrene-actin (Pyr-actin), and myosin subfragment 1 (S1) were prepared in Dr. Cremo's lab. MLCK N1-75 was expressed and purified using the method described above. Pyr-actin was prepared by isolating rabbit skeletal muscle actin and labeling with pyrene at cys-374 (Criddle *et al.*, 1985). The cys-374 pyrene is a useful probe because it is located in the myosin binding site on the actin filament. As the pyrene fluorescence is quenched upon myosin binding, pyrene fluorescence measurements can be used to measure the rate and extent of myosin binding and release. S1 was prepared by isolating smooth muscle myosin from gizzard and digesting with V8 protease (Ikebe & Hartshorne, 1985).

### **Stopped-flow Spectroscopy**

Experiments were done in 150mM KCl, 4mM MgCl<sub>2</sub>, 2mM EGTA, 1mM DTT, 25mM imidazole, pH 7.0 at 25°C using a Hi-Tech stopped-flow spectrophotometer with a mercury lamp. Pyrene fluorescence was excited at 365nm, and the emission was detected after passing through a KV 399 cutoff filter. For the control, 0.25μM Pyr-actin was rapidly mixed with 0.25μM S1 and the fluorescence change was observed. For the experimental trial, 0.25μM Pyr-actin was pre-mixed with 2μM MLCK N1-75 and then mixed with 0.25μM S1 and the fluorescence change was observed. All listed concentrations represent final values after mixing. The results shown are an average of three shots for each trial (Fig. 3).

## Results

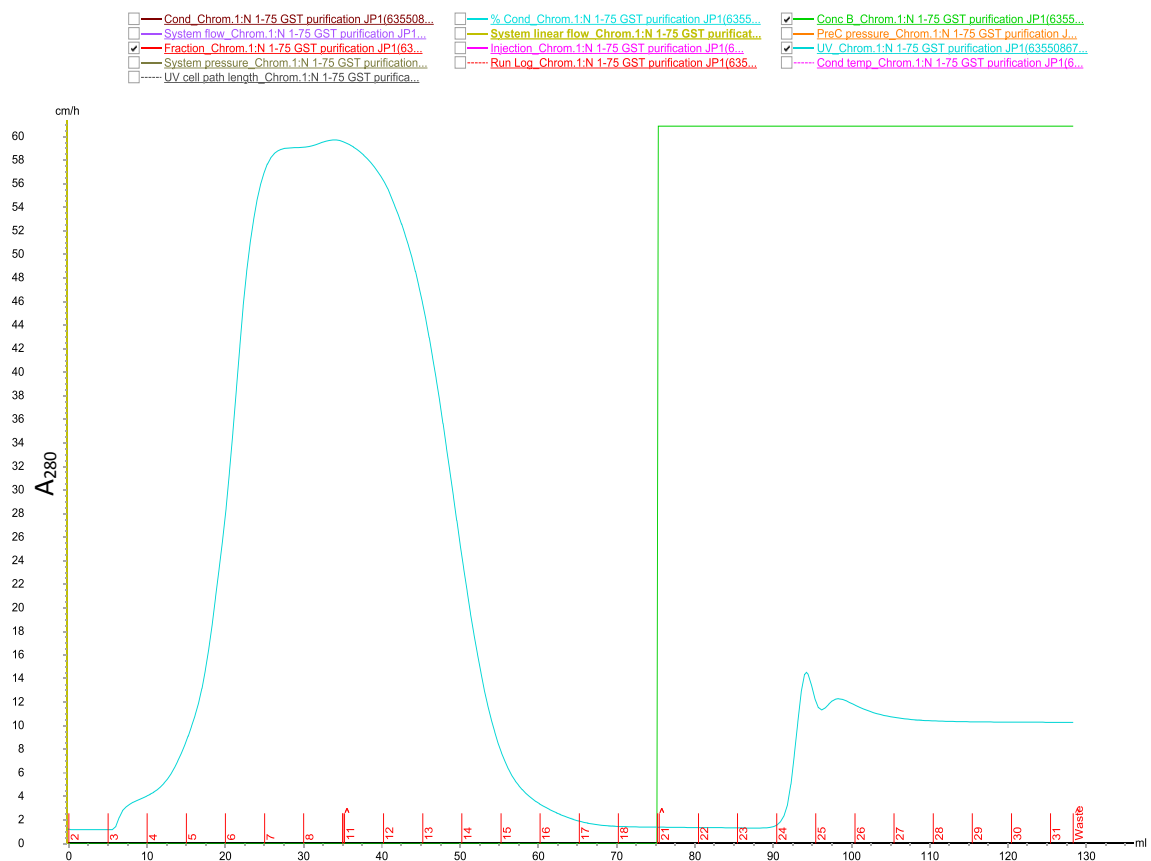


**Figure 2a. FPLC of N1-75 GST on GST 16/10 column**

50ml of cell extract containing MLCK was loaded onto the GST 16/10 column. The binding buffer was phosphate buffered saline, and the elution buffer was 50mM Tris-HCl, 10mM glutathione, and 5mM DTT. The column flow rate was set to 2 ml/min.

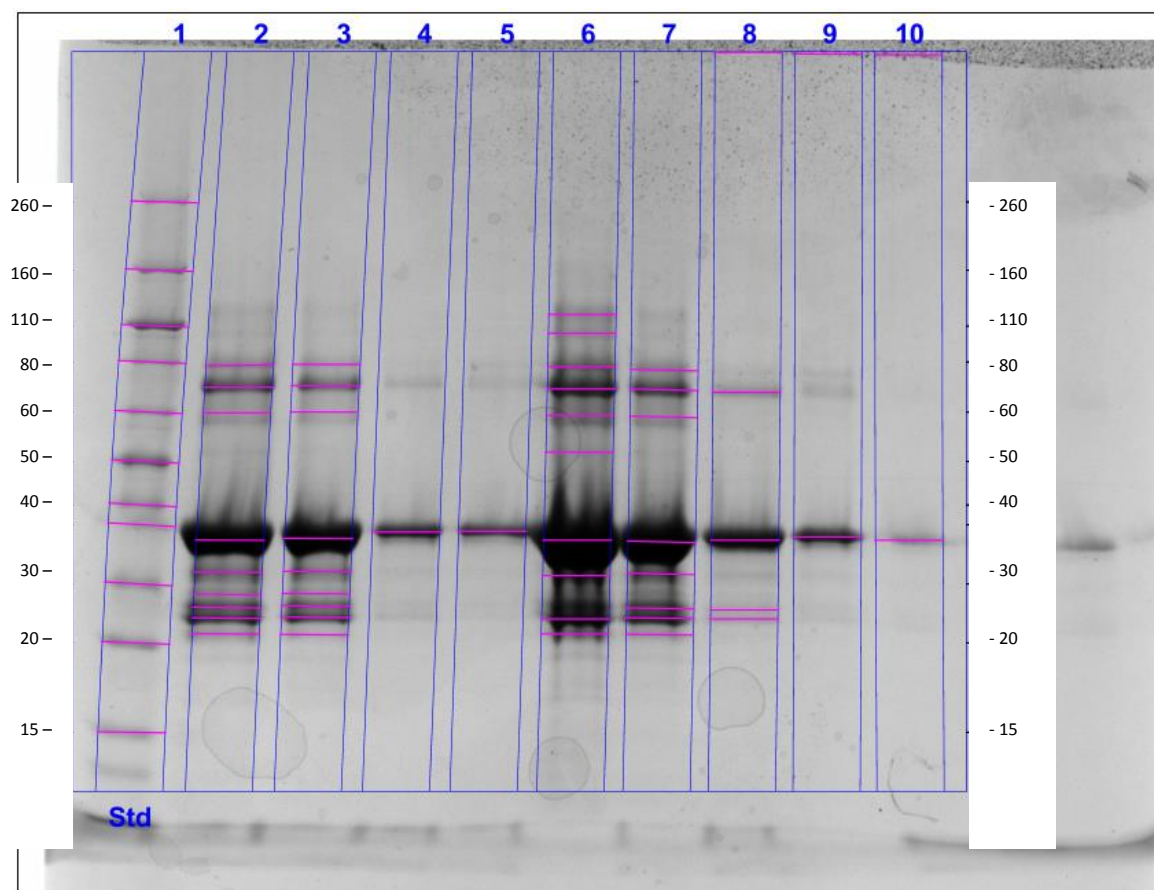


**Figure 2b. SDS-PAGE results for fractions 24-27 from FPLC**

Lanes 2-5 contain 10µl of fractions 24, 25, 26, and 27 respectively. Lanes 6-7 contain 20µl amounts of fractions 24, 25, 26, and 27 respectively. Lane 1 contains the molecular weight marker. All of the fractions show prominent bands at approximately 37kDa.

**Table 3. Initial crystallization setups observed to have favorable parameters**

Observations in the most promising initial screens approximately five weeks after the date of setup.

<b>Well #</b>	<b>Salt</b>	<b>Buffer</b>	<b>Precipitant</b>	<b>Observation</b>
Crystal Screen 2: #28	None	None	1.6M Sodium citrate tribasic dehydrate, pH 6.5	Slight spherulites and microcrystals
Crystal Screen 2: #32	0.1M NaCl	0.1M HEPES, pH 7.5	1.6M Ammonium sulfate	Slight spherulites
Crystal Screen 2: #37	None	0.1M HEPES, pH 7.5	10% w/v Polyethylene glycol 8,000 8% v/v Ethylene glycol	Slight spherulites
Crystal Screen 2: #38	None	0.1M HEPES, pH 7.5	20% w/v Polyethylene glycol 10,000	Phase separation and slight spherulites
Crystal Screen 2: #48	None	0.1M BICINE, pH 9.0	2% v/v 1,4-Dioxane 10% w/v Polyethylene glycol 20,000	Slight spherulites and needles

**Table 4. Formulations for optimized crystallization setups**

The parameters of these optimized plates were based on what appeared most likely to induce crystal growth in the initial screens (Table 3).

<b>Plate ID#</b>	<b>Salt with concentration range</b>	<b>Buffer with pH range</b>	<b>Precipitant with concentration range</b>
N75-GST 6	None	0.1M HEPES, pH 6.5-8.0	Polyethylene glycol (PEG) 5000, 10-25%
N75-GST 7	None	0.1M HEPES, pH 6.5-8.0	PEG 8000, 10-25%
N75-GST 8	None	0.1M HEPES, pH 6.5-8.0	PEG 20000, 10-25%
N75-GST 9	NaCl, 1M	0.1M HEPES, pH 6.5-8.0	Ammonium sulfate, 1-2M
N75-GST 10	NaCl, 0.05-0.3M	0.1M HEPES, pH 6.5-8.0	Ammonium sulfate, 1.5M

**Table 5. Optimized crystallization setups observed to have favorable parameters**  
 Observations in the most promising optimized screens approximately two to three weeks after the date of setup.

Plate ID#: Well #	Salt	Buffer	Precipitant	Observation
N75-GST 6: #10	None	0.1M HEPES, pH 7.0	20% Polyethylene glycol (PEG) 5000	Light precipitation and slight spherulites
N75-GST 6: #16	None	0.1M HEPES, pH 7.5	20% PEG 5000	Light precipitation and slight spherulites
N75-GST 7: #8	None	0.1M HEPES, pH 7.0	12% PEG 8000	Light precipitation and microcrystals
N75-GST 7: #18	None	0.1M HEPES, pH 7.5	25% PEG 8000	Slight spherulites and microcrystals
N75-GST 8: #23	None	0.1M HEPES, pH 8.0	22% PEG 20000	Slight spherulites
N75-GST 9: #5	0.1M NaCl	0.1M HEPES, pH 6.5	1.8M Ammonium sulfate	Light precipitation and slight spherulites
N75-GST 9: #6	0.1M NaCl	0.1M HEPES, pH 6.5	2.0M Ammonium sulfate	Light precipitation and slight spherulites
N75-GST 10: #24	0.3M NaCl	0.1M HEPES, pH 8.0	1.5M Ammonium sulfate	Slight spherulites

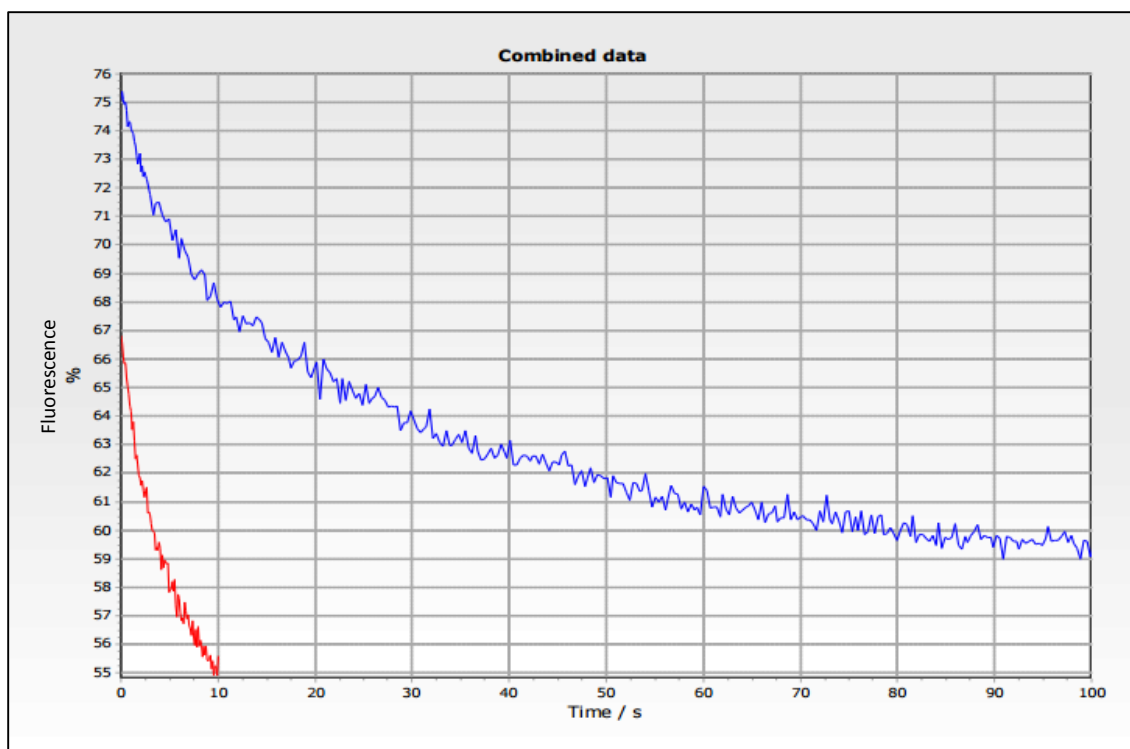


**Figure 3. N-75 binds to actin filaments and reduces the rate of S1 binding to actin.** 0.25 $\mu$ M S1 was mixed with 0.25 $\mu$ M Pyr-actin (red transient) and with 0.25 $\mu$ M Pyr-actin, 2 $\mu$ M MLCK N1-75 (blue transient). All concentrations are after mixing.  $k_{\text{obs}}$  for S1 binding in the absence of N-75 was 0.22 s $^{-1}$ . With N-75 pre-mixed with pyr-actin,  $k_{\text{obs}}$  for S1 binding was 0.035 s $^{-1}$ .

## Discussion

The purification of MLCK N1-75 from the cell lysate was successful as shown in Figure 2. In Figure 2a, fractions 24-27 from the initial peak after the glutathione elution buffer was run through the GSTPrep FF 16/10 column. Figure 2b shows that the fractions each contained protein that was 37kDa in size, consistent with the known size of the MLCK N1-75-GST construct. Therefore, these fractions were collected and pooled. The UV absorbance beyond fraction 27 is caused by the presence of glutathione from the glutathione elution buffer.

After the purified protein was placed into the initial crystallization screens, five individual setups were selected based on light microscope observations of the protein's interaction with the well reagent (Tab. 3). In all of these setups, spherulites were observed. Microcrystals, phase separation, and small needles were also observed in individual setups. The trends found in the parameters of these five setups were used to formulate the optimized crystallization plates (Tab. 4). 0.1M HEPES with a pH around 7.5 was seen to be most ideal for crystal growth, so the optimized plates all used 0.1M HEPES within a pH range of 6.5 to 8.0. Plates N75-GST 6, 7, and 8 used varying concentrations and lengths of polyethylene glycol because it was found to be the most common ideal precipitant. Plates N75-GST 9 and 10 used ammonium sulfate as the precipitant and sodium chloride as an added salt because these reagents were also observed to induce the growth of spherulites.

Table 5 shows the most promising results after two to three weeks of allowing the protein to equilibrate against the optimized formulations. These selected setups were observed to contain slight formations of spherulites, microcrystals, or both. These

observations are promising in terms of overall crystal growth; however, none of the optimized setups show evidence of single crystal formation.

Overall, crystallization of MLCK N1-75 has not yet been successful. The fact that crystallization is an empirical process makes it difficult to predict the best parameters for crystallization. Even with the perfect parameters, crystallization can take well over three weeks for certain proteins. Future experiments should take into consideration the parameters outlined in Table 5. Further optimization consisting of minor changes in the parameters may lead to crystal growth. Future trials should also attempt to crystallize MLCK N1-75 after achieving higher protein concentration and removing the GST tag because, then, the protein sample would be more pure and more susceptible to crystallization. The initial crystal screens also showed some promising observations for reagents buffered at a pH of 9.0, so future experiments should attempt to crystallize MLCK N1-75 at more alkaline conditions in BICINE or TRICINE buffer with precipitants such as polyethylene glycol.

Figure 3 shows the results of the transient kinetic experiments. When  $0.25\mu\text{M}$  S1 was added to  $0.25\mu\text{M}$  Pyr-actin alone, the rate of fluorescence decrease ( $k_{\text{obs}} = 0.22$ ) was much higher than when S1 was added to  $0.25\mu\text{M}$  Pyractin pre-mixed with  $2\mu\text{M}$  MLCK N1-75 ( $k_{\text{obs}} = 0.035$ ). These results indicate that the presence of MLCK N1-75 in solution with actin slows down the rate of S1 binding to actin. The implication is that actin, S1, and MLCK N1-75 interactions follow the scheme shown in Figure 4 below. Essentially, MLCK N1-75 appears to share a binding site with S1 for actin. MLCK N1-75 must dissociate from this binding site before S1 can interact with actin; therefore, the rate of S1 binding is slowed when MLCK N1-75 is in solution with actin. It was not possible to

repeat this experiment due to abnormalities in the quality of proteins in later trials which resulted in irregular transients. Regardless, this experiment serves as a starting point for more transient kinetics experiments with MLCK N1-75. Future experiments should attempt to repeat the trials described here and also use varying concentrations of MLCK N1-75 to assess if there is a corresponding variation in the rates of fluorescence decrease.

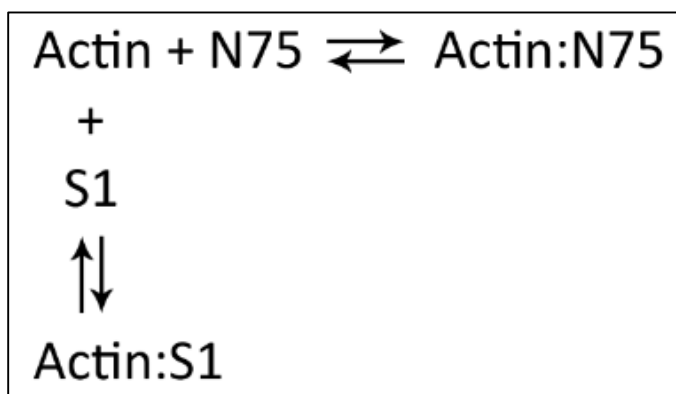


**Figure 4. Actin interactions with S1 and MLCK N1-75**

This scheme outlines how MLCK N1-75 and S1 may share the same binding site on actin. It explains why the presence of MLCK N1-75 in solution with actin decreases the rate of actin binding to S1.

## References

- Adelstein RS and Klee CB. (1981). Purification and characterization of smooth muscle myosin light chain kinase. *J. Biol. Chem.* 256(14), 7501-7509.
- Criddle AH, Geeves MA, Jeffries T. (1985). The use of actin labeled with N-(1-pyrenyl)iodoacetamide to study the interaction of actin with myosin subfragments and troponin/tropomyosin. *Biochem. J.* 232(2), 343-349.
- Hong F, Haldeman BD, Jackson D, Carter M, Baker JE, Cremo CR. (2011). Biochemistry of smooth muscle myosin light chain kinase. *Arch. Biochem. Biophys.* 510, 135-146.
- Ikebe M and Hartshorne DJ. (1985). Proteolysis of smooth muscle myosin by *Staphylococcus aureus* protease: preparation of heavy meromyosin and subfragment 1 with intact 20000-dalton light chains. *Biochemistry.* 24, 2380-2387.
- Leguillette R, Laviolette M, Bergeron C, Zitouni N, Kogut P, Solway J, Kachmar L, Hamid Q, Lauzon A-M. (2009). Myosin, transgelin, and myosin light chain kinase: expression and function in asthma. *Am. J. Respir. Crit. Care Med.* 179, 194-204.
- McPherson A and Gavira JA. (2014). Introduction to protein crystallization. *Acta Cryst.* F70, 2-20.
- Smith L and Stull JT. (2000). Myosin light chain kinase binding to actin filaments. *FEBS Lett.* 480, 298-300.
- Smith L, Su X, Lin P, Zhi G, and Stull JT. (1999). Identification of a novel actin binding motif in smooth muscle myosin light chain kinase. *J. Biol. Chem.* 274(41), 29433-29438.
- Yuan ZG, Saphirstein RJ, Yamin R, Suki B, Morgan K. (2014). Aging impairs smooth muscle-mediated regulation of aortic stiffness: a defect in shock absorption function?. *Am. J. Physiol. Heart. Circ. Physiol.* 307, H1252-H1261.